Original Article

J Korean Soc Radiol 2019;80(3):466-476
https://doi.org/10.3348/jksr.2019.80.3.466
pISSN 1738-2637 / eISSN 2288-2928

대한영상의학회지

Morphologic Evaluation of Primary Non-Small Cell Lung Cancer by 3 Tesla MRI with Free-Breathing Ultrashort Echo Time and Radial T1-Weighted Gradient Echo Sequences: A Comparison with CT Analysis

원발성 비소세포폐암의 자유 호흡 초단에코시간과 방사형 T1 강조영상 경사에코연쇄를 이용한 3T MRI에서의 형태학적 평가: CT 분석과의 비교

Hyunji Lee, MD[1], EunHee Choi, PhD[2], Myoung Kyu Lee, MD[3], Yu Zhang, MD[1], Woocheol Kwon, MD[1]*

Departments of [1]Radiology, [3]Internal Medicine, Wonju Severance Christian Hospital, Yonsei University Wonju College of Medicine, Wonju, Korea
[2]Richard A. and Susan F. Smith Center for Outcomes Research in Cardiology, Department of Medicine, Beth Israel Deaconess Medical Center, Harvard Medical School, Boston, MA, USA

Received July 12, 2018
Revised September 19, 2018
Accepted October 18, 2018

***Corresponding author**
Woocheol Kwon, MD
Department of Radiology, Wonju Severance Christian Hospital, Yonsei University Wonju College of Medicine, 20 Ilsan-ro, Wonju 26426, Korea.

Tel 82-33-741-1467
Fax 82-33-732-8281
E-mail wckwon@yonsei.ac.kr

ORCID iDs
Woocheol Kwon
https://orcid.org/0000-0003-0397-4364
Hyunji Lee
https://orcid.org/0000-0002-0187-336X

Purpose To evaluate morphologic features of primary non-small cell lung cancer using 3 Tesla MRI with free-breathing compared with CT.

Materials and Methods Thirty-six patients were enrolled. A 64-channel multidetector CT and 3 Tesla MRI with ultrashort echo time pointwise encoding time reduction with radial acquisition (PETRA) and radial volumetric interpolated breath-hold examination (VIBE) were compared in size, shape, margin, internal characteristics, and tumor interface of primary tumor.

Results There were no significant differences in tumor size between CT and either PETRA or radial VIBE ($p = 0.054$ and $p = 0.764$, respectively). Kappa (κ) statistics of shape, margin, and internal characteristics were respectively κ = 0.86, 0.65, 0.77 on PETRA and κ = 0.93, 0.84, 0.83 on radial VIBE compared with CT. PETRA and radial VIBE revealed clearer interface compared with CT ($p = 0.000$ and $p < 0.000$, respectively). Radial VIBE showed higher frequency of clear interface (94.4%) than PETRA (88.9%). MRI did not show significantly clear interface which was lo-

cated in lung base (p = 0.363 on PETRA and p = 0.175 on radial VIBE) compared with CT.
Conclusion MRI with PETRA and radial VIBE sequences can be a feasible method to evaluate morphologic features of primary non-small cell lung cancer compared with CT.

Index terms Magnetic Resonance Imaging; Carcinoma, Non-Small-Cell Lung; Diagnostic Imaging

INTRODUCTION

MRI is a radiation-free imaging modality that provides higher contrast resolution compared with CT; however, when it comes to lung, it requires long acquisition times due to low proton density and increased motion artifacts (1, 2). Conventional MRI of the lung can be performed with breath-holding, which limits the spatial resolution during the study (3). Some sequences, such as ultrashort echo (pointwise encoding time reduction with radial acquisition; PETRA) images of lung can be obtained three-dimensional (3D) images with an isotropic resolution of 1mm less than 3 minutes (4). Also optimized free-breathing 3D radial ultrashort echo time whole lung imaging was proven feasibility comparable with CT (5). Another sequence, radial 3D T1-weighted gradient echo (volumetric interpolated breath-hold examination; VIBE), enables patients to breathe freely during the scan; however, there had been no research targeted for lung nodule assessment with contrast enhancement (6, 7). The purpose of this study was to evaluate morphologic features of primary non-small cell lung cancer using 3 Tesla MRI with free-breathing compared with CT.

MATERIALS AND METHODS

STUDY POPULATION

The study was approved by the Institutional Review Board and the local ethics committee (IRB No. CR318078). All subjects provided written informed consent.

Initially, 42 patients (32 men and 10 women) with solid lung nodule or mass were prospectively enrolled between August 2015 and July 2016 at a single institution. Cases were reviewed by retrospective interpretation of prospectively acquired data.

The primary lung cancers were confirmed either by CT-guided or trans-bronchial lung biopsy. Among these cases, those with proven primary non-small cell carcinoma were selected. Three patients were pathologically diagnosed with small cell carcinoma. Another patient had proven lung metastasis due to malignant melanoma, and 2 patients had proven primary squamous cell carcinoma without demonstrable lung nodules, but with small endobronchial lesions. These 6 patients were excluded from the study. Finally, a total of 36 patients (26 men, 72.2%; 10 women, 27.8%; mean age, 71.6 ± 10.2 years; range, 44 to 90 years) were included in the analysis. Reported pathologies included 22 squamous cell carcinomas, 13 adenocarcinomas, and one pleomorphic carcinoma (Fig. 1). Among them, 7 patients underwent operation after imaging studies and tumors were resected, with pathologically confirmed whether pleural invasion was present or not.

Fig. 1. Flow chart illustrating patient selection. Among 42 patients with solid lung nodules or masses that were prospectively enrolled, 6 were excluded, resulting in a total of 36 patients with non-small cell lung cancer that were included in the study.

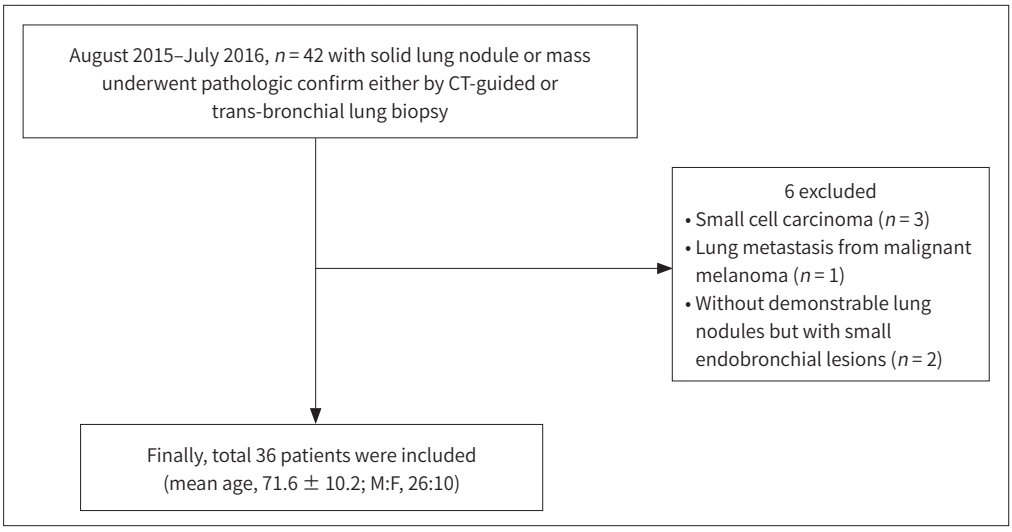

CT AND MRI PROTOCOL

A 64-channel multidetector CT scanner (Brilliance 64, Philips Medical Systems, Cleveland, OH, USA) was used for cancer staging before any treatment plans were initiated in the patients. Patients underwent 3 Tesla MRI system (MAGNETOM Skyra, Siemens, Erlangen, Germany) with a 60-channel body coil with PETRA and radial VIBE sequences were used for cancer staging before any treatment plans were initiated in the patients. The median interval between CT and MRI was 19.5 days (mean interval, 21.0 days; ranging from 0 to 49 days). CT images were acquired during inspiratory breath-hold in the supine position using a 64-channel multidetector CT scanner with the following parameters: tube voltage, 120-kV; tube current, 80 (pre) and 120 (post)-mAs; slice thickness, 2.5 mm; rotation time, 0.5 second; collimation, 0.625 mm; and 512 × 512 matrix, with field of view of 340 mm. MRI was performed in the supine position. First, T2-weighted imaging axial, T1-weighted imaging axial, T2 half-Fourier acquisition single-shot turbo spin-echo axial, T1-fat-suppressed T1-weighted imaging axial, and contrast-enhanced T1-weighted imaging axial with fat suppression were obtained in the order mentioned with the patients' arms beside their trunk. Subsequently, the patients' arms were raised to eliminate strong signals from the arms. Patients breathed freely during the scan without respiratory gating. Contrast-enhanced PETRA was performed, and radial VIBE was subsequently performed. Table 1 shows MRI sequences and acquisition time in order of acquisition.

The free-breathing PETRA image, at an isotropic resolution of 0.99 mm, was obtained in 6 minutes 2 seconds using the following parameters: repetition time (TR) = 3.59 msec; echo time (TE) = 0.07 msec; flip angle 6°; radial views = 80000; field of view = 380 mm^3; and matrix size = 384 mm^3. The parameters for free-breathing radial 3D fat-suppressed VIBE imaging with isotropic resolution of 0.9 mm were as follows: TR = 3.36 msec; TE = 1.66 msec; flip angle 5°; radial views = 853; field of view = 260 × 260 mm; matrix size = 288 × 288; total acquisition time = 5 minutes 22 seconds.

Table 1. MRI Protocol and Acquisition Time in Order of Acquisition

Pulse Sequence	Repetition Time (msec)	Echo Time (msec)	Slice Thickness (mm)	Field of View (mm)	Matrix Size (mm)	Time (min:sec)
Axial T2WI	117.0	88.0	7.0	370 × 370	256 × 256	6:33*
Axial T1WI	746.0	29.0	7.0	370 × 370	256 × 256	4:48*
Axial T1WI-fs	750.0	5.5	7.0	370 × 370	256 × 256	6:12*
Axial Gd-En T1WI-fs	654.0	36.0	7.0	370 × 370	256 × 256	3:55*
Coronal Gd-En T1WI-fs	684.0	34.0	5.0	380 × 380	256 × 256	5:58*
Gd-En PETRA	3.59 FA: 6	0.07	0.99	380 × 380 × 380	384 × 384 × 384	6:02
Gd-En radial VIBE	3.36 FA: 5	1.66	0.9	260 × 260	288 × 288	5:22

*Indicates electrocardiography-gated sequences, so acquisition times are subject to patients' RR interval.
fs = fat suppression, Gd-En = gadolinium-enhanced, PETRA = point-wise encoding time reduction with radial acquisition, T1WI = T1-weighted imaging, T2WI = T2-weighted imaging, VIBE = volumetric interpolated breath-hold examination

Both CT and MRI were acquired with contrast enhancement. As CT contrast agent, iohexol 350 (Bonorex 350; Central Medical Service Co. Ltd, Seoul, Korea) was used at an injection rate of 2.5 cc/second. For MRI, patients received 0.1 mmol/kg body weight of gadoteridol (ProHance; Bracco Imaging, Milano, Italy) as contrast material at an injection rate of 1.5 cc/second. Enhanced images were sequentially obtained immediately after contrast material injection.

IMAGE ASSESSMENT

All measurements were processed in Digital Imaging and Communication in Medicine format from a Picture Archiving and Communication System (Centricity Radiology RA 1000; General Electric Healthcare, Barrington, IL, USA) to a personal computer for analysis. Lung imaging was evaluated by consensus by two radiologists (reader 1, 15 years' clinical experience; reader 2, 5 years' clinical experience). To eliminate recall bias, the image was blinded and was assessed a total of 3 times for 3 months through blinded ordinal scoring.

Tumor size, shape, margin, internal characteristics, and tumor interface with adjacent structures were evaluated. The primary tumor size was measured and categorized as tumor (T) staging via eighth edition of the tumor-node-metastasis (TNM) classification of lung cancer (8). The longest diameter of the tumor was obtained on axial lung settings (width 1600, level -600). Other T descriptor such as relationship with pleura, diaphragm, and great vessel was not considered.

Tumor shape was graded as round, oval, or irregular. The tumor margin was rated as well- or ill-defined. The internal characteristics of the tumor were evaluated on the enhanced image, and rated as homogeneous or heterogeneous when internal necrosis, calcification, or bubble-like lucency leads to heterogeneous texture (9, 10). Internal necrosis is defined as heterogeneous low attenuation or signal intensity without cavitation on enhanced CT or MRI. Calcification is defined as high attenuated foci on CT and corresponding signal void on MRI. Bubble-like lucency is defined as intratumoral air attenuation or signal intensity. Finally, the tumor interface with adjacent structures was graded as "clear" when the image was well delineated or "obliterated" when it was not delineated, including adjacent organ invasion. Tumor interface analysis was categorized as lesion location. Tumor location was categorized as lobar anatomy, and lower lobe lesion was subdivided to lung base when the lesion was con-

tact with diaphragm.

STATISTICAL METHODS

The size values were assessed via paired *t*-test. Kappa (κ) statistics were used to analyze the agreement between CT and PETRA, and CT and radial VIBE values of tumor shape, margin, internal characteristics, and tumor interface. Agreement was considered slight if the κ-values range below 0.20, fair if they were between 0.21–0.40, moderate if they were between 0.41–0.60, substantial if they were between 0.61–0.80, and almost perfect if the value was greater than 0.81 (11). Pearson correlation coefficient was performed to evaluate the relationships between the CT measurements with PETRA and radial VIBE. The McNemar's test was used to assess the statistical significance of any difference among the CT with PETRA and radial VIBE in terms of shape, margin, internal characteristics, and tumor interface subcategorized by lesion location. A *p*-value of < 0.05 was considered statistically significant. All statistical analyses were performed using SAS 9.4 version (SAS Institute Inc., Cary, NC, USA).

RESULTS

The distribution of tumors from CT imaging was categorized according to T stage: T1b (*n* = 1), T1c (*n* = 9), T2a (*n* = 8), T2b (*n* = 1), T3 (*n* = 7), and T4 (*n* = 10). The average size of the tumors was 41.7 mm (range, 14–80 mm) on CT. There were no significant differences in average size between the two MRI sequences (42.9 mm for PETRA, $p = 0.054$; 41.8 mm for radial VIBE, $p = 0.764$) compared with CT values.

Table 2 shows tumor distribution by its location. Total 18 tumors (50.0%) were located in upper lobes and 18 tumors (50.0%) were located in lower lobes. Among lower lobe tumors, 6 tumors (16.7% of total tumors) were located in lung base.

Regarding the shape and margin between CT and MRIs, there was higher correspondence on radial VIBE with almost perfect agreement (shape, $\kappa = 0.93$ and margin, $\kappa = 0.84$; respectively) than PETRA which showed almost perfect agreement on shape ($\kappa = 0.86$) and substantial on tumor margin ($\kappa = 0.65$) compared with CT. The internal characteristics of tumor homogeneity or heterogeneity in radial VIBE had more corresponding features than those of PETRA. The κ-values of comparison between CT and the two MRI modalities were substantial on PETRA ($\kappa = 0.77$) and almost perfect on radial VIBE ($\kappa = 0.83$) (Table 3).

Table 2. Distribution of the Tumors According to Location

Location	Number of Tumors (%)
RUL	9 (25.0)
RML	0
RLL*	8 (22.2)
LUL	9 (25.0)
LLL*	4 (11.1)
Lung base	6 (16.7)

*Indicates tumors located in lower lobes, but with no contact with diaphragm. Tumors displaying contact with diaphragm in imaging were classified as being in the lung base.
LLL = left lower lobe, LUL = left upper lobe, RLL = right lower lobe, RML = right middle lobe, RUL = right upper lobe

Internal components of the tumors with heterogeneous internal characteristics are shown in Table 4. Necrosis was seen in 13 tumors (36.1% of total tumor) on CT and among them, 76.9% was seen in PETRA and 92.3% was seen in radial VIBE. Six intratumoral calcifications were shown on CT and half of them were seen in PETRA and radial VIBE. Bubble-like lucency of tumor was seen in 13 cases on CT, and 84.6% and 92.3% of them were shown in PETRA and radial VIBE, respectively (Fig. 2). The *p*-value of internal necrosis, calcification, and bubble-like lucency between CT and respective MRI sequences were above 0.05.

Both MRI sequences revealed overall clearer tumor interface compared with CT ($p = 0.000$ for PETRA; $p < 0.000$ for radial VIBE); 20 cases graded as obliterated on CT were revealed as clear on MRI (Fig. 3). Between the MRI sequences, the higher frequency of clear tumor inter-

Table 3. Agreement between Free-Breathing PETRA and Radial VIBE Compared to CT, as κ-Values*

	Shape	Margin	Internal Characteristics
PETRA	0.86	0.65	0.77
Radial VIBE	0.93	0.84	0.83

*Agreement was considered slight if the κ-values were below 0.20, fair if they were between 0.21–0.40, moderate if they were between 0.41–0.60, substantial if they were between 0.61–0.80, and almost perfect if they were greater than 0.81.
κ = Kappa, PETRA = pointwise encoding time reduction with radial acquisition, VIBE = volumetric interpolated breath-hold examination

Table 4. Internal Characteristics of Tumors Observed on CT, PETRA, and Radial VIBE

	CT	PETRA (% of CT Finding, *p*-Value)	Radial VIBE (% of CT Finding, *p*-Value)
Necrosis	13	10 (76.9, 0.250)	12 (92.3, 1.000)
Calcification	6	3 (50.0, 0.250)	3 (50.0, 0.250)
Bubble-like lucency	13	11 (84.6, 0.500)	12 (92.3, 1.000)

Internal necrosis is defined as inhomogeneous low attenuation or signal intensity without cavitation on enhanced CT or MRIs. Calcification is defined as high attenuated foci on CT and corresponding signal void on MRIs. Bubble-like lucency is defined as intratumoral air attenuation or signal intensity.
PETRA = pointwise encoding time reduction with radial acquisition, VIBE = volumetric interpolated breath-hold examination

Fig. 2. Contrast-enhanced axial chest CT (A), PETRA (B), and radial VIBE (C) images from a 44-year-old woman with adenocarcinoma in right upper lobe. Arrows indicate intratumoral bubble-like lucency.
PETRA = pointwise encoding time reduction with radial acquisition, VIBE = volumetric interpolated breath-hold examination

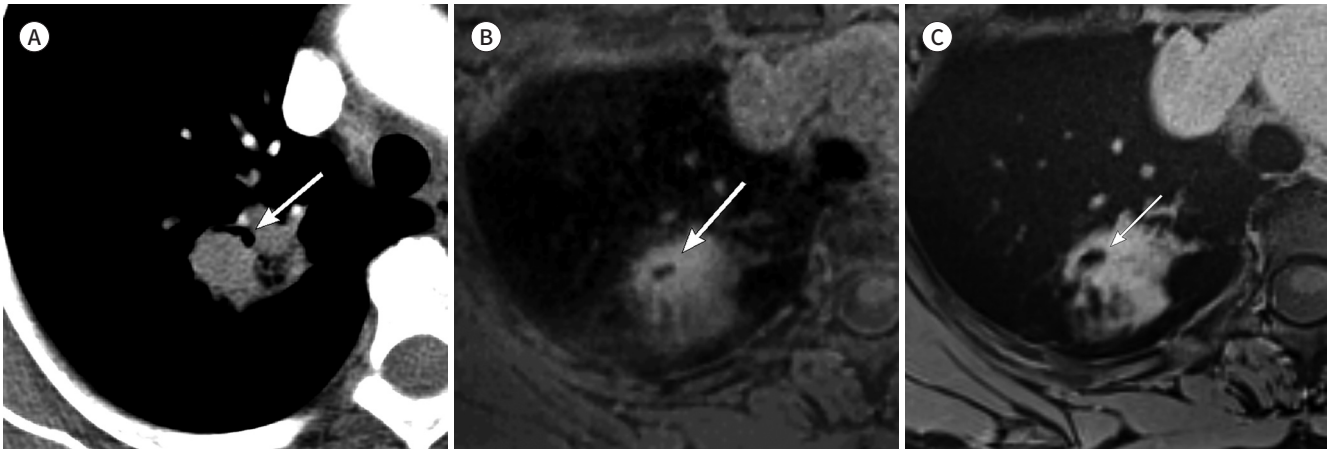

Fig. 3. Contrast-enhanced axial chest CT (A), PETRA (B), and radial VIBE (C) images from a 78-year-old man with squamous cell carcinoma in left lower lobe. In (A), the mass's interface (arrow) shows obliterated relationship with adjacent chest wall on CT. However, on MRI, the tumor interface with the pleura (arrows, B, C) is clear. This is well-recognized in (C) rather than (B). This mass underwent operation and was proven to have no parietal pleural invasion.
PETRA = pointwise encoding time reduction with radial acquisition, VIBE = volumetric interpolated breath-hold examination

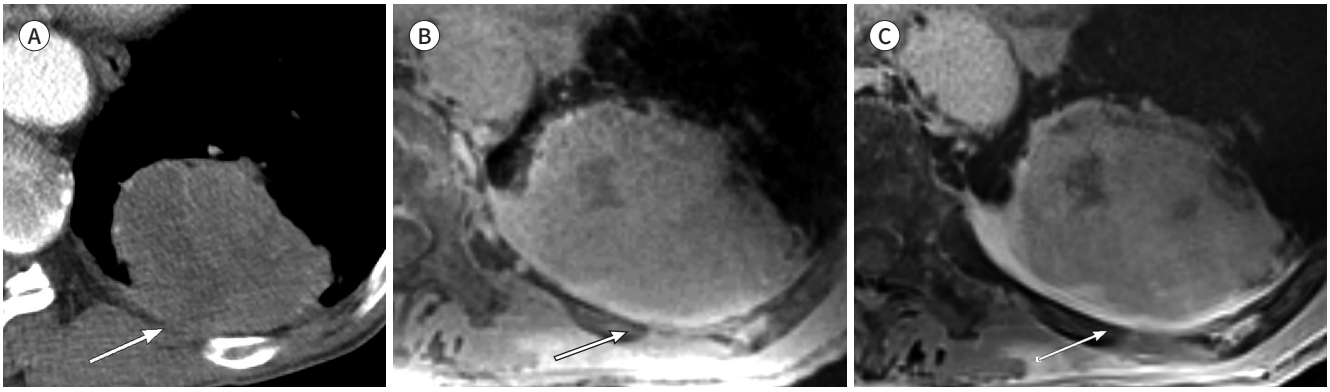

Table 5. Number of Patients Categorized According to Tumor Interface

CT	PETRA			Radial VIBE		
	Clear	Obliterated	*p*-Value	Clear	Obliterated	*p*-Value
Upper lobe (*n* = 18)						
Clear	7	1	0.021	8	0	-
Obliterated	9	1	0.021	10	0	-
Lower lobe (*n* = 12)						
Clear	4	0	-	4	0	-
Obliterated	8	0	-	8	0	-
Lung base (*n* = 6)						
Clear	1	1	0.625	2	0	0.500
Obliterated	3	1	0.625	2	2	0.500

Indicates tumors located in lower lobes, but not contact with diaphragm. Tumors displaying contact with the diaphragm on imaging were classified as being in the lung base.
PETRA = pointwise encoding time reduction with radial acquisition, VIBE = volumetric interpolated breath-hold examination

face was seen at radial VIBE (34/36, 94.4%) than PETRA (32/36, 88.9%). However, by analyzing subdivided tumor groups in locations, lung base lesions were not statistically significant in tumor interfaces in MRI sequences compared with CT (Table 5). Two cases of obliterated tumor interface in radial VIBE was seen only in lung base tumors (Fig. 4).

Among 7 patients who underwent surgery was proven as no pleural invasion in 3 cases and visceral pleural invasion beyond the elastic layer in 3 cases. All these tumors were seen as clear tumor interface on both PETRA and radial VIBE. One case of invading into the visceral pleural surface was in right lung base and had obliterated feature both on PETRA and radial VIBE.

DISCUSSION

The role of MRI in depicting the details of pulmonary structures is limited due to lack of tissue compared with other organs because of short T2*, with rapid decay of the signal in the lungs, which is the most challenging organ for MRI techniques (1). However, some sequences

Fig. 4. Coronal reformatted images of contrast-enhanced chest CT (A), PETRA (B), and radial VIBE (C) images from a 65-year-old man with adenocarcinoma in right lower lobe base. An irregular nodule (arrow) with contact with the adjacent diaphragm is apparent in (A). However the nodule (arrows) is not apparent in (B, C). PETRA = pointwise encoding time reduction with radial acquisition, VIBE = volumetric interpolated breath-hold examination

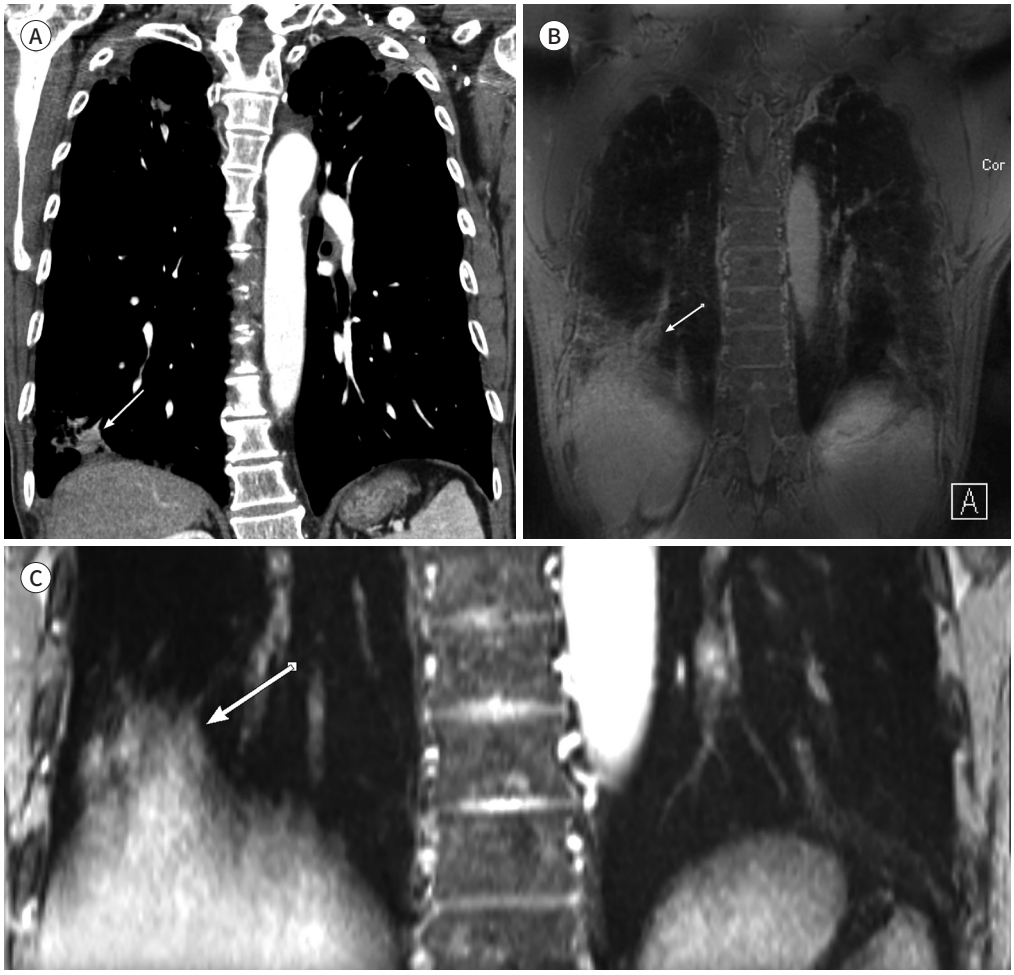

that can overcome shortcomings in tissue contrast of the lung have been developed, enabling the detection and characterization of lung nodules, and also of pulmonary embolism (12, 13). With the introduction of contrast material during the scan, tumor necrosis, mediastinal invasion, pleural reaction, and carcinomatosis can be more evident (14). Therefore, MRI can be superior to CT for discriminating tumors and determining whether they are resectable (15). Acquisition of lung signal by ultrashort TE sequences with 3D radial projection enables free-breathing with reduced noise (16). This can be applicable to patients who experience side effects from CT contrast materials or who are uncooperative with requisite breath-holding during CT scans. Submillimeter axial PETRA and radial VIBE images can be reconstructed to coronal and sagittal images without additional scans. It can lead to more detailed tumor evaluation in thin slices compared with conventional MRI images.

In our study, there were no overall significant differences in images used for assessing tumors in size, shape, margin, and internal characteristics between breath-hold CT and free-breathing MRI. Furthermore, there was no significant difference of tumor size and internal

characteristics seen on PETRA and radial VIBE images compared with CT. All cases except for lung base lesions in radial VIBE provided clear tumor interfaces in this study; this is crucial for patients not only for staging, but also to ensure precise evaluation of tumor spread before surgery (17). There were only 7 cases with pathologically proven resected pleura to determine true invasion that can be compared with image findings, but the sample size was too small to statistically evaluate. Further study about comparing radiologic and pathologic finding of pleura with more cases will be helpful.

Results of the tumor interface largely depended on tumor location. When tumors were located in the lung bases, characterization was difficult in MRI compared with CT images due to respiratory motion. Diaphragmatic movement, as well as increased noise with respiratory-gated MRI sequences, can be causative. In this case, we recommend performing MRI with patients in breath-hold. In addition, image quality is inferior during expiration or shallow breathing (18). Therefore, we recommend acquiring images with breath-holding at the end-inspiratory state when possible (19). It is difficult to assess tumor with associated collapse consolidation on CT. Ultrashort TE sequences of MRI had no additional role in assessment of the tumor within consolidations. In these cases, further research can be expected using dynamic contrast enhancement or other MRI sequences.

There were several limitations to this study, the first of which was its small sample size. Second, the average size of the tumors was somewhat larger than that of tumors encountered in routine clinical practice. We enrolled patients who underwent both CT and MRI. However, due to clinical circumstances, including issues regarding medical insurance, and clinical issues such as patients' and clinicians' need for additional information about the tumor, the pool of eligible lung cancer patients was limited. Lung cancer patients with smaller tumor size or easily resectable tumors did not undergo MRI and, therefore, were naturally excluded from this study. Lastly, only half of the calcification seen on CT is detected on MRI, although the sample size is small. There is limitation in intratumoral calcification detection on MRI.

In conclusion, 3T MRI with free-breathing and PETRA and radial VIBE sequences is a feasible method to assess primary tumor size, internal characteristics, and tumor interface of non-small cell lung cancer compared with CT. Moreover, it enables free breathing in patients with primary non-small cell lung cancer, and may be an alternative modality to CT for patients who experience side effects from CT contrast material, or when technical difficulties involving adequate breath-holding are encountered.

Conflicts of Interest

The authors have no potential conflicts of interest to disclose.

REFERENCES

1. Dournes G, Grodzki D, Macey J, Girodet PO, Fayon M, Chateil JF, et al. Quiet submillimeter MR imaging of the lung is feasible with a PETRA sequence at 1.5 T. *Radiology* 2015;276:258-265
2. Kurihara Y, Matsuoka S, Yamashiro T, Fujikawa A, Matsushita S, Yagihashi K, et al. MRI of pulmonary nodules. *AJR Am J Roentgenol* 2014;202:W210-W216
3. Stolzmann P, Veit-Haibach P, Chuck N, Rossi C, Frauenfelder T, Alkadhi H, et al. Detection rate, location, and size of pulmonary nodules in trimodality PET/CT-MR: comparison of low-dose CT and Dixon-based MR imaging. *Invest Radiol* 2013;48:241-246

4. Grodzki DM, Jakob PM, Heismann B. Ultrashort echo time imaging using pointwise encoding time reduction with radial acquisition (PETRA). *Magn Reson Med* 2012;67:510-518
5. Johnson KM, Fain SB, Schiebler ML, Nagle S. Optimized 3D ultrashort echo time pulmonary MRI. *Magn Reson Med* 2013;70:1241-1250
6. Chandarana H, Heacock L, Rakheja R, DeMello LR, Bonavita J, Block TK, et al. Pulmonary nodules in patients with primary malignancy: comparison of hybrid PET/MR and PET/CT imaging. *Radiology* 2013;268:874-881
7. Chandarana H, Block TK, Rosenkrantz AB, Lim RP, Kim D, Mossa DJ, et al. Free-breathing radial 3D fat-suppressed T1-weighted gradient echo sequence: a viable alternative for contrast-enhanced liver imaging in patients unable to suspend respiration. *Invest Radiol* 2011;46:648-653
8. Amin MB, Edge SB, Greene FL, Byrd DR, Brookland RK, Washington MK, et al. *AJCC cancer staging manual*. 8th ed. New York: Springer International Publishing 2017
9. Liu Y, Wang H, Li Q, McGettigan MJ, Balagurunathan Y, Garcia AL, et al. Radiologic features of small pulmonary nodules and lung cancer risk in the national lung screening trial: a nested case-control study. *Radiology* 2018;286:298-306
10. Kuriyama K, Tateishi R, Doi O, Higashiyama M, Kodama K, Inoue E, et al. Prevalence of air bronchograms in small peripheral carcinomas of the lung on thin-section CT: comparison with benign tumors. *AJR Am J Roentgenol* 1991;156:921-924
11. Kundel HL, Polansky M. Measurement of observer agreement. *Radiology* 2003;228:303-308
12. Dournes G, Menut F, Macey J, Fayon M, Chateil JF, Salel M, et al. Lung morphology assessment of cystic fibrosis using MRI with ultra-short echo time at submillimeter spatial resolution. *Eur Radiol* 2016;26:3811-3820
13. Bannas P, Bell LC, Johnson KM, Schiebler ML, François CJ, Motosugi U, et al. Pulmonary embolism detection with three-dimensional ultrashort echo time MR imaging: experimental study in canines. *Radiology* 2016;278:413-421
14. Biederer J, Mirsadraee S, Beer M, Molinari F, Hintze C, Bauman G, et al. MRI of the lung (3/3)-current applications and future perspectives. *Insights Imaging* 2012;3:373-386
15. Purandare NC, Rangarajan V. Imaging of lung cancer: implications on staging and management. *Indian J Radiol Imaging* 2015;25:109-120
16. Gai ND, Malayeri A, Agarwal H, Evers R, Bluemke D. Evaluation of optimized breath-hold and free-breathing 3D ultrashort echo time contrast agent-free MRI of the human lung. *J Magn Reson Imaging* 2016;43:1230-1238
17. Landwehr P, Schulte O, Lackner K. MR imaging of the chest: mediastinum and chest wall. *Eur Radiol* 1999;9:1737-1744
18. Schwenzer NF, Seith F, Gatidis S, Brendle C, Schmidt H, Pfannenberg CA, et al. Diagnosing lung nodules on oncologic MR/PET imaging: comparison of fast T1-weighted sequences and influence of image acquisition in inspiration and expiration breath-hold. *Korean J Radiol* 2016;17:684-694
19. Semelka RC, Cem Balci N, Wilber KP, Fisher LL, Brown MA, Gomez-Caminero A, et al. Breath-hold 3D gradient-echo MR imaging of the lung parenchyma: evaluation of reproducibility of image quality in normals and preliminary observations in patients with disease. *J Magn Reson Imaging* 2000;11:195-200

대한영상의학회지

원발성 비소세포폐암의 자유 호흡 초단에코시간과 방사형 T1 강조영상 경사에코연쇄를 이용한 3T MRI에서의 형태학적 평가: CT 분석과의 비교

이현지[1] · 최은희[2] · 이명규[3] · 장 옥[1] · 권우철[1*]

목적 원발성 비소세포폐암의 형태학적 특징을 자유 호흡하는 3 Tesla 자기공명영상(magnetic resonance imaging; 이하 MRI)과 전산화단층촬영술(computed tomography; 이하 CT)에서 비교 평가하였다.

대상과 방법 36명의 환자를 대상으로 하였다. 64통로 다중검출 CT와 3 Tesla MRI로 촬영한 초단에코시간(pointwise encoding time reduction with radial acquisition; 이하 PETRA)과 방사형 용적보간호흡정지(radial volumetric interpolated breath-hold examination; 이하 radial VIBE) 연쇄 영상을 촬영하여 폐암 병변의 크기, 모양, 변연, 내부 특성, 그리고 종양 경계면 에 대해 비교하였다.

결과 종양의 크기는 CT와 PETRA 또는 radial VIBE간 유의한 차이를 보이지 않았다(각 p = 0.054와 p = 0.764). 모양, 변연, 내부특성의 일치도는 PETRA에서 각각 κ = 0.86, 0.65, 0.77이었고 radial VIBE에서 κ = 0.93, 0.84, 0.83였다. PETRA와 radial VIBE는 CT에 비해 더욱 정밀한 종양 계면을 보여주었다(각 p = 0.000과 p < 0.000). Radial VIBE (94.4%)는 PETRA (88.9%) 보다 더 명확한 계면 구분을 보여주었다. MRI는 폐 기저부에 위치한 경우 CT에 비해 명확한 계면을 유의하게 보여주지 못하였다(PETRA에서 p = 0.363와 radial VIBE에서 p = 0.175).

결론 PETRA와 radial VIBE를 이용한 MRI는 원발성 비소세포암의 형태학적 평가에 CT와 비교해서 실현 가능한 방법이다.

연세대학교 원주의과대학 원주세브란스기독병원 [1]영상의학과, [3]내과,
[2]Richard A. and Susan F. Smith Center for Outcomes Research in Cardiology, Department of Medicine, Beth Israel Deaconess Medical Center, Harvard Medical School